Journal of Instrumentation

TECHNICAL REPORT • **OPEN ACCESS**

A newly observed phenomenon in the characterisation of SiPM at cryogenic temperature

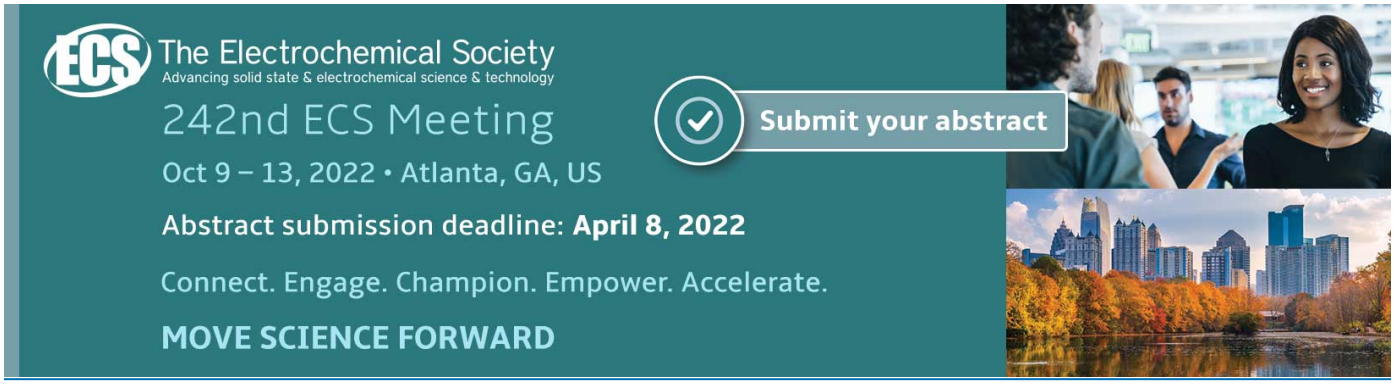

Published by IOP Publishing for Sissa Medialab

Received: *May 21, 2021*
Revised: *July 17, 2021*
Accepted: *October 4, 2021*
Published: *October 22, 2021*

TECHNICAL REPORT

A newly observed phenomenon in the characterisation of SiPM at cryogenic temperature

M. Guarise,[a,b,*] **M. Andreotti,**[b] **R. Calabrese,**[a,b] **A. Cotta Ramusino,**[b] **V. Cicero,**[c,d] **M. Fiorini,**[a,b] **T. Giammaria,**[a,b] **I. Lax,**[d] **E. Luppi,**[a,b] **A. Minotti,**[a,b] **E. Montagna,**[c,d] **A. Montanari,**[d] **L. Patrizii,**[d] **M. Pozzato**[d] **and L. Tomassetti**[a,b]

[a] *Dipartimento di Fisica e Scienze della Terra, Università di Ferrara, Via G. Saragat 1, I-44122, Ferrara, Italy*
[b] *INFN Ferrara, Via G. Saragat 1, I-44122, Ferrara, Italy*
[c] *Dipartimento di Fisica e Astronomia, Via C. Berti Pichat 6/2, I-40127, Bologna, Italy*
[d] *INFN Bologna, Via C. Berti Pichat 6/2, I-40127, Bologna, Italy*

E-mail: marco.guarise@fe.infn.it

Abstract: In this article we report a novel phenomenon that we observed while evaluating the performances of different models of silicon photomultiplier detectors at liquid nitrogen temperature. Bursts of consecutive events, characterized by a rate that is about 100 times that of the single-event uncorrelated dark counts, are generated within the SiPMs, resulting in an overall increase of the dark current. We observed these bursts in the vast majority of the tested SiPM models manifactured by Hamamatsu Photonics K.K. This observation is part of an effort to fully characterise the behaviour of SiPMs at cryogenic temperature. The investigation of this phenomenon, of which a first attempt is presented in this article, can impact future production and selection of models for both high energy physics and industrial applications.

Keywords: Detectors for UV, visible and IR photons; Photon detectors for UV, visible and IR photons (solid-state); Photon detectors for UV, visible and IR photons (solid-state) (PIN diodes, APDs, Si-PMTs, G-APDs, CCDs, EBCCDs, EMCCDs, CMOS imagers, etc); Cryogenic detectors

*Corresponding author.

https://doi.org/10.1088/1748-0221/16/10/T10006

2021 JINST 16 T10006

Contents

2021 JINST 16 T10006

1 Introduction

Silicon photomultipliers (SiPMs), sometimes referred as multi-pixel proportional counters (MPPCs), are photosensors consisting of a large matrix of single-photon avalanche diodes (SPADs) operating in the Geiger-Müller regime. The matrix behaves like a single detector, producing a macroscopic current when hit by one or several photons [1]. With respect to other photosensors, SiPMs are characterised by a good robustness, high sensitivity and dynamic range, and magnetic field immunity. Moreover, their reduced cost and size allow to fill large surfaces with high granularity sensors. For such reasons, these detectors have being increasingly preferred to other traditional photosensors in the last years [2–5]. The applications of SiPMs span a very wide range that includes particle physics and astronomy [6–9], industry and technology [10, 11], and the medical sector [12, 13].

In low photon count applications, the main drawback of SiPM detectors is the relatively high dark count rate (DCR) at room temperature ($\sim 100\,\mathrm{kHz/mm^2}$), which is dominated by the thermal generation of carriers in the silicon junction that mimic the absorption of a photon in the sensor [1]. This issue can be overcome by cooling the SiPMs at cryogenic temperatures, thus lowering the Boltzmann factor by many orders of magnitude, resulting in the inter-band tunnel effect being the main contributor to the DCR [1]. Nevertheless, a thorough investigation of the behaviour of the SiPMs at cryogenic temperatures is lacking, and unexplained phenomena could still be observed. In this article we present experimental results concerning an unexpected correlated noise that we have found in several SiPMs models operated at low temperature. The paper is organised as follows: in section 2 we present the experimental set-up and the sensors that have been used for these studies, in section 3 we describe the protocol and results of our measurements, and in section 4 we discuss the possible implications and further investigation that could be performed on this topic.

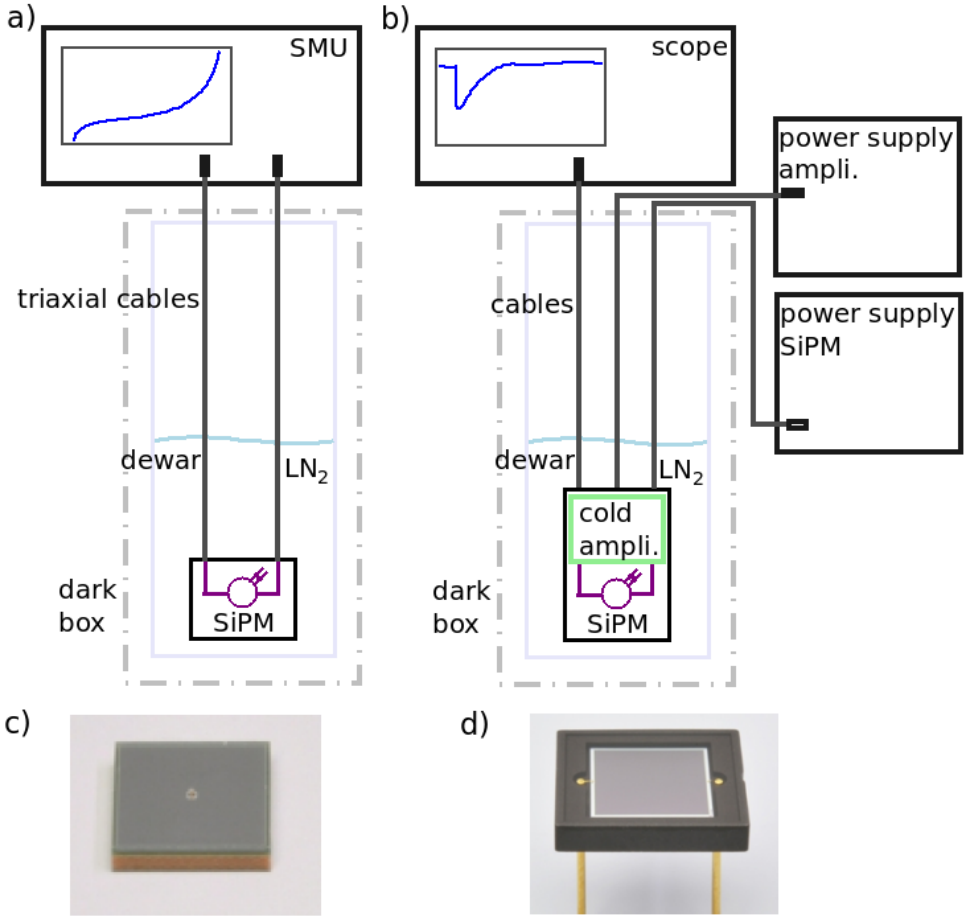

Figure 1. a) Sketch of the set-up used for IV-curve measurements; b) Sketch of the set-up used for dark count rate measurements; c) and d) are different examples of tested SiPMs: the first is a surface mount type with a hole wire bonding connections, while the latter has a ceramic packaging with a lateral wire bonding.

2 Experimental set-up for cryogenic characterisation of SiPMs

In order to characterise the SiPM detectors at cryogenic temperatures, the first step consists in the measurement of the current-voltage characteristic curve (IV), which allows to quantify the breakdown voltage (V_{BD}) and quenching resistor (R_Q). The former parameter is particularly important because it enables the definition of the working point of the sensor in terms of applied voltage, while the latter impacts the shape of the recorded signals. As numerous works demonstrate, the R_Q increases when the SiPM is cooled down at LN2 temperature, while the V_{BD} decreases [14–18].

Once the V_{BD} and the R_Q are determined, the following step consists in counting the signals produced by the SiPM, with an applied voltage that exceeds V_{BD} by a few volts (V_{OV}), and in absolute darkness. These signals include the already mentioned dark counts, as well as correlated events shortly-following an avalanche. When these events happen in the same SPAD they are known as afterpulse (AP), while we refer to them as cross-talk (CT) when they happen in a different SPAD. Primary dark signals, CT and AP events, are distinguishable by studying their amplitude and intrinsic time, as we will show later in this article.

2021 JINST 16 T10006

2.1 Tested SiPM devices

As previously mentioned, the SiPM models that have been tested for this study were produced by Hamamatsu Photonics K.K. (HPK). The main characteristics of the sensors that are not covered by nondisclosure agreement with the vendor are listed in table 1. For many of these devices more details can be found in HPK SiPM catalog. The active area of all the tested SiPMs is 36 mm^2. The number of samples that have been tested for each (#) model is reported in the last column.

Table 1. Characteristics of the different models of SiPMs that have been tested for this study. * =custom splits produced for DUNE experiment based on the 13360 chip with a low quenching resistors which are ~ 35 Ω and ~ 50 Ω at room temperature for the 50 µm and the 75 µm pitch, respectively. [1] = surface mount type; [2] = hole wire bonding; [3] = standard lateral wire bonding; [4] = through silicon via bonding. [a] = see description in the text. Different examples of the package of these SiPMs are shown in figure 1c) and d).

Model	***Pitch***	N_{cells}	***Package***	***Connections***	***Window***	***Resin thickness***	***#*** [a]
HPK 13360-6050LRQ*	50 µm	14331	SMT[1]	HWB[2]	silicone resin	150 µm	14
HPK 13360-6075LRQ*	75 µm	6364	SMT[1]	HWB[2]	silicone resin	150 µm	20
HPK 13360-6025CS	25 µm	57600	Ceramic	LB[3]	silicone resin	400 µm	2
HPK 13360-6050CS	50 µm	14331	Ceramic	LB[3]	silicone resin	400 µm	3
HPK 13360-6075CS	75 µm	6400	Ceramic	LB[3]	silicone resin	400 µm	2
HPK 13360-6050VE	75 µm	14331	SMT[1]	TSV[4]	epoxy resin	100 µm	2
HPK 14160-6050HS	50 µm	14331	SMT[1]	HWB[2]	silicone resin	150 µm	2

2.2 Experimental apparatus

The sketches of the used experimental set-up are shown in figure 1. A 20 dm^3, large-aperture dewar, filled with liquid nitrogen, provides the cryogenic environment for the measurement. The dewar is placed into a custom dark box covered by polyurethane-coated black fabric to shield the sensors from external light. The different instrumentation used for the IV curve and DCR measurements are shown in figure 1a) and 1b) respectively. For the IV curve, a source meter unit (SMU[1]) is connected to the cathode and anode of the tested SiPM through two triaxial cables in order to reduce the electronic noise. The SMU provides the voltage supply for the sensor and at the same time it measures the output current, producing the IV curve of the diode. When measuring the DCR we instead couple the SiPM anode to a custom cryogenic AC amplifier[2] to produce a signal that is readable directly at the oscilloscope.[3] The voltage across the SiPM is ensured by a stabilised DC power supply,[4] while another DC power supply guarantees the amplifier operation.[5] In either case, the characterisation of the SiPM starts 30 minutes after the immersion in liquid nitrogen, to ensure full thermalisation of the sensor.

The oscilloscope used for the DCR measurement was set to the *fast frame* acquisition mode, in which for every trigger a recorded waveform is stored in a temporary buffer before being saved to disk. This enables relatively long data acquisitions with deadtimes that are negligible with respect

[1]Keithley Sourcemeter 2450.
[2]Custom amplifier designed by INFN Bologna. Bandwidth> 300 MHz; gain~ 15 µV/fC.
[3]Tektronix MSO oscilloscope 6 series.
[4]TTI EX354T DC power supply.
[5]Keysight E3648A dual power supply.

2021 JINST 16 T10006

to the expected DCR (~Hz). Typically, we collect a few thousands of 4 µs waveforms, sampled in 5000 points each (samplig rate = 1.25 GS/s) setting an analogic input bandwidth at 20 MHz. This corresponds to about 1 h of data taking. Other acquisition parameters of the oscilloscope are a 50 Ω input load and a 0.5 photoelectrons (p.e.) trigger threshold on the negative slope of the signal.

Two examples of waveforms recorded setting a trigger threshold at −3.5 mV (−0.5 p.e.) are shown in figure 2. In the first one (figure 2a), a single dark count signal is present, while in the second one (figure 2b), a cross-talk (CT) between two different SPADS produced a peak with double amplitude. In addition to that, an after pulse (AP) event happening during the recharging of the cell, results in a smaller delayed peak.

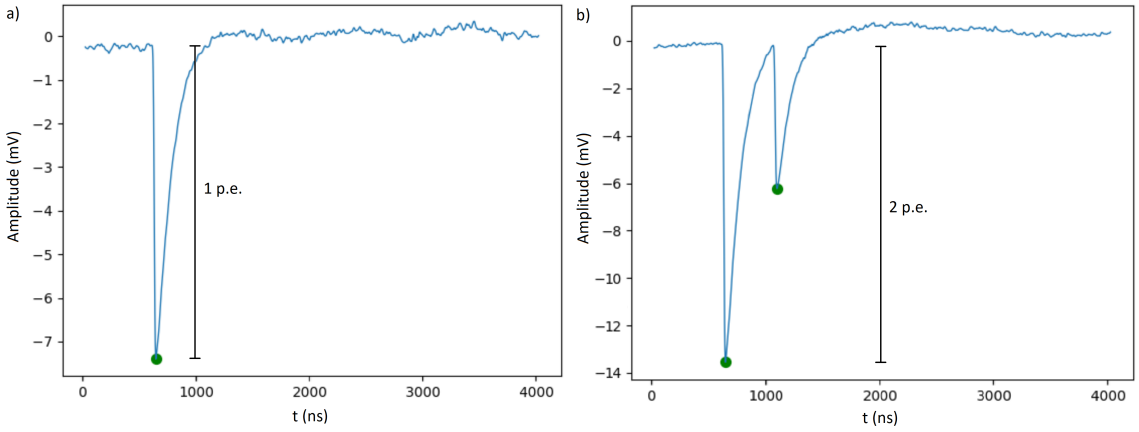

Figure 2. Examples of recorded waveform; the x axis is the time, while the y axis is the SiPM output signal in mV. The green points are identified as peaks. a) This waveform shows a single dark signal; b) this waveform shows a CT and an AP event.

The oscilloscope stores the acquired data in two comma-separated values (csv) files: one containing the waveforms; and the other storing the relative time of each trigger with respect to the previous one. These files are then processed offline with a dedicated software that extrapolates the peaks and computes the values of DCR, as well as the probability of AP and CT events.

2.3 Offline analysis

The offline analysis is performed by means of two python scripts. The first one, or *waveform_analyzer*, isolates the single waveforms, and computes the timestamp of each data point by combining the information from the two oscilloscope output files. It then proceeds to identify the peaks, corresponding to local minima of the waveform (see figure 2), and to compute their time and amplitude by subtracting the local waveform baseline (i.e. the average value of the pre-trigger data). The list of selected peaks with their times and amplitudes is then processed by a second algorithm, the *peak_analyzer*, which is used to produce the results and plots related to the SiPM characterisation that are shown in this article.

3 Measurements and results

Figure 3, produced by the *peak_analyzer*, shows the distribution of selected events in terms of peak amplitude and time delay Δt between consecutive peaks, for one of the tested SiPMs (HPK

2021 JINST 16 T10006

13360-6075LRQ) operated at +3 V of overvoltage. In the figure we can clearly see a cluster of events with a 1 p.e. amplitude and a Δt of the order of a second, corresponding to the primary dark signals. In this figure, we can also recognize a second smaller distribution of events at very short Δt ($[10^{-8}$–$10^{-6}]$ s), corresponding to the AP and events with an amplitude of 2 or more p.e., corresponding to the CT. In addition to that, another group of events with a 1 p.e. amplitude, but a Δt of the order of [0.1–10] ms, is clearly distinguishable from the dark signals cluster. These events correspond to quick trains, or bursts, of correlated events, the origin of which is still to be understood. The presence of such bursts is clearly visible also from figure 4, which shows the amplitude and time trend distribution of the events. The average Δt between peaks drops in correspondence of one burst occurring, slowly coming back to previous values as the burst ends (figure 4b). The bursts are also identifiable as peaks in the timestamp distribution (figure 4a).

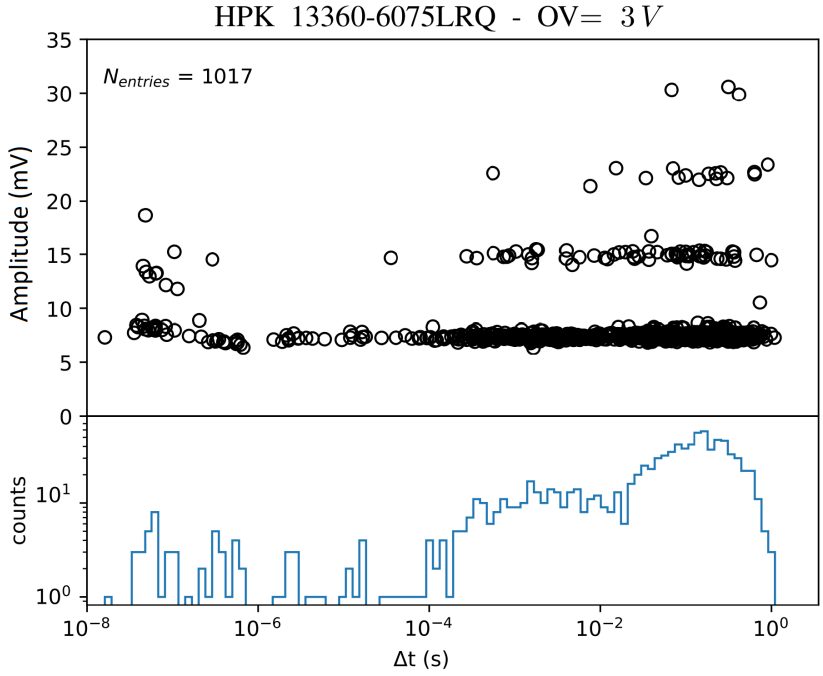

Figure 3. Time-delay (Δt) and amplitude (A) distribution of identified peaks produced by the *peak_analyzer*. Primary dark signals are clustered at $\Delta t \sim 0.1$ s and $A = 1$ p.e. ($\sim 7\,mV$); after pulses have much shorter Δt ($[10^{-8}$–$10^{-6}]$ s); while cross-talk events have $A > 1$ p.e. Events from bursts resemble primary dark signals, but have a shorter Δt ([0.1–10] ms).

In figure 5b), the same amplitude-Δt distribution of figure 3 is shown for the SiPM model HPK 13360-6050CS operated at +3 V of overvoltage. In this case, only the standard DCR population is visible, and the population due to bursts is absent, as these trains of events do not occur for this SiPM model. A similar plot can be produced for the previous sensor (HPK 13360-6075LRQ), by removing offline the bursts as shown in figure 5a). This is achieved by the *peak_analyser* with a dedicated algorithm that identifies chains of events with short Δt, and allows to separate events belonging to different clusters (bursts and DCR).

By tagging and isolating the bursts and the first event of each, we can study these trains of events. We identified some common features of the bursts: first, they tend to start with a relatively

2021 JINST 16 T10006

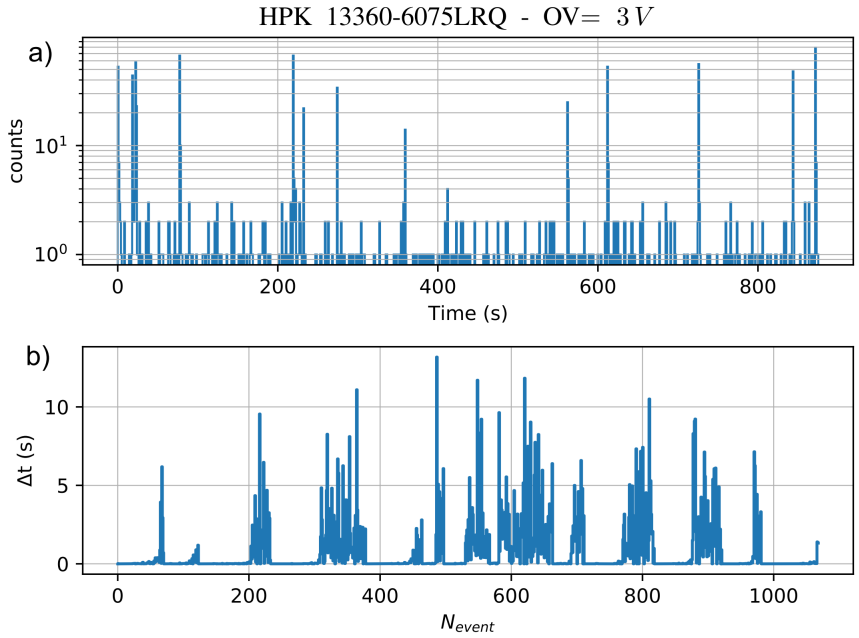

Figure 4. a) histogram of the absolute time (timestamp) of single peaks. b) Δt between events vs event ID.

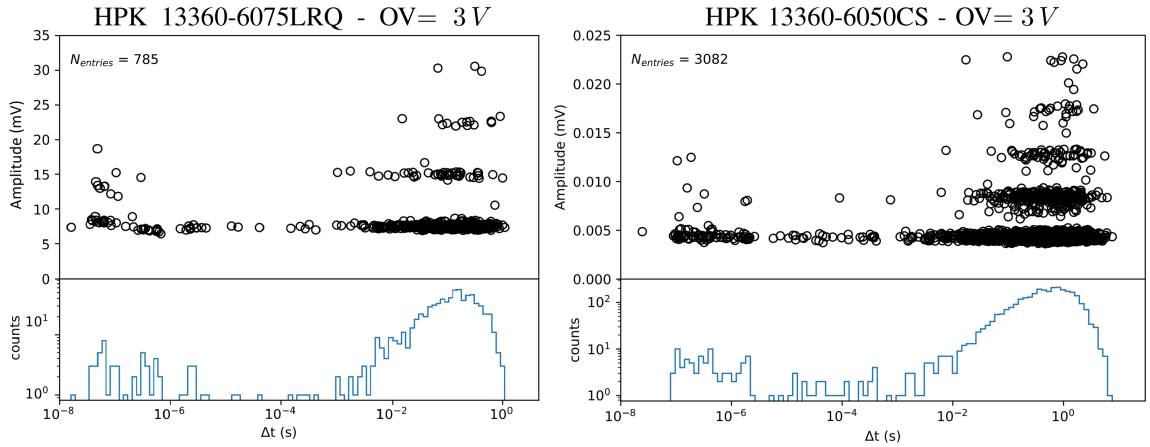

Figure 5. Time-delay (Δt) and amplitude distribution of identified peaks produced by the *peak_analyzer*. Figure a) shows the SiPM model HPK 13360-6075LRQ, where the events from bursts are removed offline while figure b) shows the distribution of another SiPM model (HPK 13360-6050CS), that does not present any burst.

high-amplitude event (≥ 4 p.e.) as shown in the histogram of figure 6; secondly the average number of events with a $[0.1 - 10]$ ms Δt contained in a burst is ~ 100 (bottom plot of figure 6); and finally they generally last for a few tenths of a second. All the peaks in the bursts are distributed around the 1 p.e. amplitude value, except for the CT and AP events, that are still present. No evidences of correlations between burst events and R_Q or V_{BD} as derived from the charachteristics IV curve of the SIPMs have been found.

The values of the measured DCR of different models of SiPM, compared to the one calculated after the offline analysis that identifies and removes burst events, are shown in the table 2. Considering

2021 JINST 16 T10006

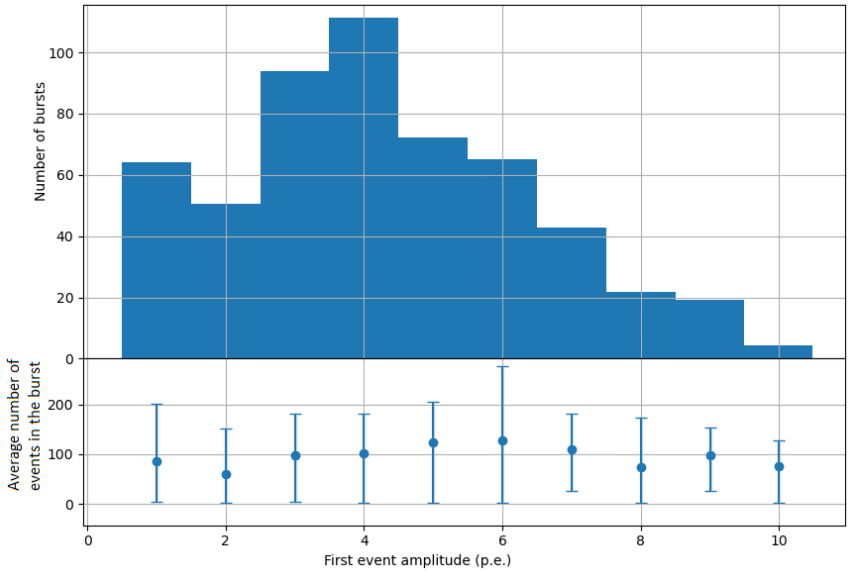

Figure 6. Number of events in a burst vs amplitude of its first event.

the whole sensors, the values of the DCR range between ~0.2 Hz and ~2 Hz and, as expected, DCR decreases always in the SiPMs that show bursts behavior. As shown in the table, the following models do not present burst events: HPK 13360-6025CS; HPK 13360-6050CS and HPK 13360-6075CS.

Table 2. Some results of the data obtained using the *peak_analyzer* algorithm. [1]tested @ OV = +3 V; [2]tested @ OV = +4 V.

Model	***Measured DCR***	***Burst events***	***DCR with offline burst removal***
HPK 13360-6050LRQ[1]	(41 ± 6) mHz/mm^2	yes	(20 ± 4) mHz/mm^2
HPK 13360-6075LRQ[1]	(49 ± 8) mHz/mm^2	yes	(20 ± 7) mHz/mm^2
HPK 13360-6025CS[2]	(7 ± 1) mHz/mm^2	no	(7 ± 1) mHz/mm^2
HPK 13360-6050CS[1]	(36 ± 1) mHz/mm^2	no	(36 ± 1) mHz/mm^2
HPK 13360-6075CS[1]	(14 ± 1) mHz/mm^2	no	(14 ± 1) mHz/mm^2
HPK 13360-6050VE[1]	(44 ± 1) mHz/mm^2	yes	(17 ± 1) mHz/mm^2
HPK 14160-6050HS[1]	(117 ± 1) mHz/mm^2	yes	(14 ± 1) mHz/mm^2

4 Discussion and conclusions

In this article we present a newly discovered phenomenon occurring in some HPK silicon photomultiplier models at liquid nitrogen temperature. Bursts of consecutive avalanche events, typically triggered by a high-amplitude event and separated by [0.1–10] ms, result in an increased total number of dark counts for the device. They differ from primary dark signals by their higher frequency and correlated nature. This phenomenon is not reported in literature yet, and neither the cause nor the underlying physical mechanism are known. Nevertheless, we developed analysis tools to isolate and study the bursts, and identified some of their common features. These bursts of events have been observed in both SiPMs with silicone or epoxy coating, with hole wire bond or through silicon via

2021 JINST 16 T10006

connections, and with different cell pitch. We did not find this behavior in the models 13360-60xxCS (where xx = 25, 50 and 75 and stands for the cell pitch in µm) which are ceramic mount SIPMs with a lateral bond and a 400µm coating silicone resin.

Currently, we are investigating the nature of these bursts, in collaboration with the vendor, by developing dedicated studies. A better understanding of such behaviour could in fact have crucial implications in the selection of models of SiPM for their numerous applications. Furthermore, these studies could lead to a better characterisation of SiPM behaviour at cryogenic temperatures.

Acknowledgments

The authors would like to thank S. Chiozzi and S. Squerzanti for the precious technical work. The authors participating in the DUNE single phase photon detection (SPPD) consortium acknowledge its support in making available the custom sensors. We would like to thank also HPK Italy for the helpful discussions. This work was partially funded by INFN and the University of Ferrara (FIR 2020).

References

[1] F. Acerbi and S. Gundacker, *Understanding and simulating SiPMs*, *Nucl. Instrum. Meth. A* **926** (2019) 61659.

[2] D. Renker, *Geiger-mode avalanche photodiodes, history, properties and problems*, *Nucl. Instrum. Meth. A* **567** (2006) 48.

[3] G. Collazuol, *The sipm physics and technology-a review*, talk given at the *International Workshop on New Photon-detectors*, LAL, Orsay, France, 13–15 June 2012.

[4] S. Gundacker and A. Heering, *The silicon photomultiplier: fundamentals and applications of a modern solid-state photon detector*, *Phys. Med. Biol.* **65** (2020) 17TR01.

[5] D. Herbert, V. Saveliev, N. Belcari, N. D'Ascenzo, A.D. Guerra and A. Golovin, *First results of scintillator readout with silicon photomultiplier*, *IEEE Trans. Nucl. Sci.* **53** (2006) 389.

[6] C. D'Ambrosio, *The Future of RICH Detectors through the Light of the LHCb RICH*, *Nucl. Instrum. Meth. A* **876** (2017) 194 [arXiv:1703.09927].

[7] DUNE collaboration, *Prospects for beyond the Standard Model physics searches at the Deep Underground Neutrino Experiment*, *Eur. Phys. J. C* **81** (2021) 322 [arXiv:2008.12769].

[8] E.J. Schioppa et al., *An innovative SiPM-based camera for gamma-ray astronomy with the small size telescopes of the Cherenkov Telescope Array*, 2016 *JINST* **11** C01038.

[9] S. Catalanotti, A.G. Cocco, G. Covone, M. D'Incecco, G. Fiorillo, G. Korga et al., *Performance of a SensL-30035-16P Silicon Photomultiplier array at liquid argon temperature*, 2015 *JINST* **10** P08013 [arXiv:1505.07261].

[10] R. Agishev, A. Comerón, J. Bach, A. Rodriguez, M. Sicard, J. Riu et al., *Lidar with SiPM: Some capabilities and limitations in real environment*, *Opt. Laser Techn.* **49** (2013) 86.

[11] A.M. Antonova and V.A. Kaplin, *SiPM timing characteristics under conditions of a large background for lidars*, *J. Phys. Conf. Ser.* **945** (2018) 012012.

[12] S. Sajedi, N. Zeraatkar, M. Taheri, S. Kaviani, H. Khanmohammadi, S. Sarkar et al., *Generic high resolution PET detector block using* 12×12 *SiPM array*, *Biomed. Phys. Eng. Express* **4** (2018) 035014.

2021 JINST 16 T10006

[13] A. Dalla Mora, L. Di Sieno, A. Behera, P. Taroni, D. Contini, A. Torricelli et al., *The SiPM revolution in time-domain diffuse optics*, *Nucl. Instrum. Meth. A* **978** (2020) 164411.

[14] A. Gola, F. Acerbi, M. Capasso, M. Marcante, A. Mazzi, G. Paternoster et al., *NUV-sensitive silicon photomultiplier technologies developed at fondazione bruno kessler*, *Sensors* **19** (2019) 308.

[15] K. Ozaki, S. Kazama, M. Yamashita, Y. Itow and S. Moriyama, *Characterization of New Silicon Photomultipliers with Low Dark Noise at Low Temperature*, 2021 *JINST* **16** P03014 [arXiv:2007.13537].

[16] T. Cervi et al., *Study of SiPM custom arrays for scintillation light detection in a Liquid Argon Time Projection Chamber*, 2017 *JINST* **12** C03007.

[17] F. Acerbi, S. Davini, A. Ferri, C. Galbiati, G. Giovanetti, A. Gola et al., *Cryogenic characterization of FBK HD near-UV sensitive SiPMs*, *Trans. Electron Devices* **64** (2017) 521.

[18] M. Ramilli, *Characterization of SiPM: Temperature dependencies*, *IEEE Nucl. Sci. Symp. Conf. Rec.* (2008) 2467.

2021 JINST 16 T10006